Heat and Mass Transfer Analysis of an unsteady Non-Newtonian Magnetohydrodynamic Fluid Flow (Semi-Analytical Solution)

AMINE EL HARFOUF[1, *], RACHID HERBAZI[2,3,4], SANAA HAYANI MOUNIR[1],
HASSANE MES-ADI[5], ABDERRAHIM WAKIF[6]
[1]Multidisciplinary Laboratory of Research and Innovation (LaMRI),
Energy, Materials, Atomic and Information Fusion (EMAFI) Team,
Polydisciplinary Faculty of Khouribga,
Sultan Moulay Slimane University,
MOROCCO

[2]Intelligent Systems and Applications Laboratory (LSIA), EMSI,
Tangier,
MOROCCO

[3]ENSAT, Abdelmalek Essaâdi University,
Tangier,
MOROCCO

[4]ERCMN, FSTT, Abdelmalek Essaâdi University,
Tangier,
MOROCCO

[5]Laboratory of Process Engineering, Computer Science and Mathematics,
National School of Applied Sciences of the Khouribga University of Sultan Moulay Slimane,
MOROCCO

[6]Faculty of Sciences Aïn Chock, Laboratory of Mechanics,
Hassan II University,
Casablanca,
MOROCCO

**Corresponding Author*

Abstract: - In the presence of a time-dependent chemical reaction, this work investigates unsteady squeezing Casson nanofluid flow and heat transfer between two parallel plates under the influence of a uniform magnetic field. Considering the effects of viscosity dissipation, heat generation from friction resulting from flow shear, Brownian motion, Joule heating, and thermodiffusion. The problem's nonlinear differential equations are solved using the Runge–Kutta (RK-4) technique and the Homotopy Perturbation technique. The excellent accuracy of the results is evident since they have been compared with other results from earlier research. In the form of graphs and tables, flow behavior under the many physical factors that are modified is also covered and well described. This work has shown that, by normalizing flow behavior, magnetic fields may be utilized to manage a variety of flows. Additionally, it is demonstrated that in every situation, the effects of positive and negative squeeze numbers on heat and mass transfer flow are opposite. Moreover, the thermophoresis parameter decreases as the concentration field increases. However, when the Brownian motion parameter is increased, the concentration profile gets better. Additionally, several other significant factors were examined. The results of this study can facilitate quicker and easier research and assist engineers.

Keywords: - Casson nanofluid, squeezing flow, Homotopy perturbation method (HPM), Runge–Kutta (RK-4), magnetic field, Brownian motion, Thermophoresis.

Received: April 22, 2023. Revised: September 25, 2023. Accepted: November 21, 2023. Published: December 31, 2023.

Nomenclature

cp	Specific heat at constant pressure
B	Magnetic field
D_T	Thermophoretic diffusion coefficient
Ha	Hartmann number
l	Distance of plate
N_t	Thermophoretic parameter
p	Pressure
S	Squeeze number
T	Fluid temperature
C	Nanofluid concentration
D_B	Brownian diffusion coefficient
E_c	Eckert number
k	Thermal conductivity
a	Rate of squeezing

Greek Symbols

θ	Dimensionless temperature
ρ	Density (kgm^{-3})
μ	Dynamic viscosity of nanofluid
σ	Electrical conductivity of nanofluid
β	Casson fluid parameter
Φ	Dimensionless concentration

1 Introduction

The many mechanical and organic applications of heat and mass transfer squeezing flow, such as polymer processing, water cooling, hydro-mechanical gear, and chemical processing equipment, have drawn a lot of attention to the field in recent years. In [1], the authors reported the first study in this field utilizing lubrication approximation. Numerous academics examined these flows for various scenarios and geometries. In their investigation, considered the effects of injection or suction at the walls when analyzing the analytical solution for the squeezing flow of viscous fluid between parallel disks, [2]. In the same context, the authors have addressed the squeezing flow across a porous surface, [3]. Also, in [4], looked at the combined impacts of heat and mass transfer in the squeezing flow between parallel plates while taking chemical reaction effects and viscous dissipation into account. Additionally, taking thermal radiation into consideration. On the other hand, they investigated the MHD nanofluid flow and heat transfer in a stretching/shrinking convergent/divergent channel, [5]. Additionally, in [6], investigated the heat transmission and nanofluid flow between two parallel plates in a spinning device.

Non-Newtonian fluids are more practical to utilize in actual industrial applications than Newtonian fluids, such as paints, tomato sauce, condensed milk, and shampoos. Non-Newtonian fluids exhibit unique characteristics that defy explanation by Newtonian theory.

The shear stress and shear rate in a Newtonian fluid have a linear relationship that passes through the origin, with the coefficient of viscosity serving as the constant of proportionality. The connection between the shear stress and the shear rate is different in a non-Newtonian fluid, though. The fluid can display viscosity in relation to time. As such, it is impossible to establish a constant viscosity coefficient. Many non-Newtonian models on various physical characteristics have been proposed to close this gap. One example of a non-Newtonian fluid used to mimic blood in arteries is the Casson fluid; its formulation may be acquired from, [7], and Casson fluid has been the subject of multiple investigations. In other work, [8], [9] have investigated the Casson fluid for both constant and oscillatory blood flow as well as the flow between two revolving cylinders. While in [10], examined the unstable Boundary Layer Flow of a Casson Fluid Due to an Impulsively Started Moving Flat Plate, they examined the constant flow of a Casson fluid in a tube, [11].

This paper addresses the squeezing flow of a two-dimensional incompressible Casson nanofluid between two parallel plates under the influence of a uniform magnetic field. It considers various factors such as viscous dissipation effect, heat generation due to friction caused by shear in the flow, Joule heating, Brownian motion, and thermophoresis effect with time-dependent chemical reaction. The research is motivated by the above investigations. Since the most significant engineering problems heat transfer equations are nonlinear, some of them may be solved numerically, while others can be solved analytically using various techniques. To get the optimum outcome, both approaches were applied in this study. Researchers in this field have used analytical techniques such as the differential

transformation method (DTM) [12], [13] Homotopy perturbation technique HPM [14], adomian decomposition method ADM [15], homotopy analysis method HAM [16], and variation of parameter method VPM [17]. The HPM, which He invented and refined, is an analytical simulation technique that does not need tiny parameters [18]. According to this approach, the answer is found by adding up an infinite series, which often converges quickly to the precise answer. Thus, the fourth order Runge–Kutta technique (RK-4) has been used as a numerical approach and HPM as an analytical method to solve the reduced ordinary differential equations in this paper.

2 Mathematical Formulation of the Problem

This work examines the heat and mass transfer in the unstable two-dimensional Casson nanofluid squeezing flow between two infinite parallel plates, as seen in Figure 1. The distance between the two plates $y = \pm h(t) = \pm l(1-at)^{\frac{1}{2}}$, where l is the initial location (when time $t = 0$) for $\alpha > 0$ the two plates are squeezed until they touch $t = 1/\alpha$ and for $\alpha < 0$ There is a separation between the two plates. It is assumed that a constant magnetic field is applied in the direction of y. Assuming a low magnetic Reynolds number, the induced magnetic field may be insignificant when compared to the applied magnetic field. As a result, the following define the electromagnetic force and the electric current:

$\vec{J} = \sigma(\vec{v}\times\vec{B})$, $\vec{F} = \vec{J}\times\vec{B}$ then $\vec{F} = \sigma(\vec{v}\times\vec{B})\times\vec{B}$.

The rheological equation of state for an isotropic flow of a Casson fluid can be expressed as, [19]:

$$\tau_{ij} = \begin{cases} 2\left(\mu_B + \frac{p_y}{\sqrt{2\pi}}\right)e_{ij}\,, \pi > \pi_c \\ 2\left(\mu_B + \frac{p_y}{\sqrt{2\pi_c}}\right)e_{ij}\,, \pi < \pi_c \end{cases} \quad (1)$$

Where τ_{ij} is the $(i,j)^{th}$ component of stress tensor, $\pi = e_{ij}e_{ij}$ represent the product of deformation components, e_{ij} indicates the deformation rate on the $(i,j)^{th}$ component, π_c indicates the critical value. The Casson fluid's dynamic plastic viscosity is represented by μ_B and p_y represents the yield stress.

The deformation rate is equal to:

$$e_{ij} = \frac{1}{2}\left(\frac{\partial u_i}{\partial x_j} + \frac{\partial u_j}{\partial x_i}\right) \quad (2)$$

For the sake of this issue, the equations controlling the Casson nanofluid flow for mass, momentum, thermal energy, and nanoparticle concentration are expressed as:

$$\frac{\partial u}{\partial x} + \frac{\partial v}{\partial y} = 0 \quad (3)$$

$$\left(u\frac{\partial u}{\partial x} + v\frac{\partial u}{\partial y}\right) = -\frac{1}{\rho_{nf}}\frac{\partial p}{\partial x} + \frac{\mu_{nf}}{\rho_{nf}}\left(1+\frac{1}{\beta}\right)* \left(2\frac{\partial^2 u}{\partial x^2} + \frac{\partial^2 u}{\partial y^2} + \frac{\partial^2 v}{\partial y \partial x}\right) - B_0^2\frac{\sigma_{nf}}{\rho_{nf}}u \quad (4)$$

$$\left(u\frac{\partial v}{\partial x} + v\frac{\partial v}{\partial y}\right) = -\frac{1}{\rho_{nf}}\frac{\partial p}{\partial y} + \frac{\mu_{nf}}{\rho_{nf}}\left(1+\frac{1}{\beta}\right)* \left(2\frac{\partial^2 v}{\partial y^2} + \frac{\partial^2 v}{\partial x^2} + \frac{\partial^2 u}{\partial y \partial x}\right) \quad (5)$$

$$\left(\frac{\partial T}{\partial t} + u\frac{\partial T}{\partial x} + v\frac{\partial T}{\partial y}\right) = \frac{k_{nf}}{(\rho c_p)_{nf}}\left(\frac{\partial^2 T}{\partial x^2} + \frac{\partial^2 T}{\partial y^2}\right) + B_0^2\frac{\sigma_{nf}}{(\rho c_p)_{nf}}u^2 + \frac{\mu_{nf}}{(\rho c_p)_{nf}}\left(1+\frac{1}{\beta}\right)* \left[4\left(\frac{\partial u}{\partial x}\right)^2 + \left(\frac{\partial u}{\partial y} + \frac{\partial v}{\partial x}\right)^2\right] + \frac{(\rho c_p)_p}{(\rho c_p)_{nf}}\left[D_B\left(\frac{\partial C}{\partial x}\frac{\partial T}{\partial x} + \frac{\partial C}{\partial y}\frac{\partial T}{\partial y}\right) + \frac{D_T}{T_\infty}\left(\frac{\partial T}{\partial x}\frac{\partial T}{\partial x} + \frac{\partial T}{\partial y}\frac{\partial T}{\partial y}\right)\right] \quad (6)$$

$$\frac{\partial C}{\partial t} + u\frac{\partial C}{\partial x} + v\frac{\partial C}{\partial y} = D_B\left(\frac{\partial^2 C}{\partial x^2} + \frac{\partial^2 C}{\partial y^2}\right) + \frac{D_T}{T_\infty}\left(\frac{\partial^2 T}{\partial x^2} + \frac{\partial^2 T}{\partial y^2}\right) - G(t)C \quad (7)$$

The boundary conditions are:

$$u = 0,\ v = v_w = \frac{dh}{dt},\ T = T_H, C = C_H\ at \quad (8)$$

$$y = h(t)$$

$$v = \frac{du}{dy} = \frac{dT}{dy} = \frac{dC}{dy} = 0 \; at \; y = 0 \qquad (9)$$

Where u and v are the velocities in the x and y directions respectively, T is the temperature, P is the pressure, σ is the electric conductivity, K is the effect thermal conductivity,C is the concentration, μ is the dynamic viscosity, D_B and D_T are the Brownian motion coefficient and the thermophoretic diffusion coefficient , T_∞ is the mean fluid temperature , $\beta = \frac{\mu_B\sqrt{2\pi_c}}{p_y}$ is the Casson fluid parameter and $G(t) = \frac{g}{(1-\alpha t)}$ is the time-dependent reaction rate.

The following dimensionless groups are introduced:

$$\begin{aligned} \eta &= \frac{y}{l(1-\alpha t)^{\frac{1}{2}}} = \frac{y}{h(t)} \\ u &= \frac{x\alpha}{2(1-\alpha t)} f'(\eta) \\ v &= -\frac{\alpha l}{2(1-\alpha t)^{\frac{1}{2}}} f(\eta) \\ \Theta &= \frac{T}{T_H} \end{aligned} \qquad (10)$$

Equations 3 through **7** are obtained by substituting the parameters, and the results yield:

$$\begin{aligned} &\left(1+\frac{1}{\beta}\right) f''''(\eta) \\ &\quad - S[\eta f'''(\eta) + f'(\eta) f''(\eta) \\ &\quad - f(\eta) f'''(\eta) + 3f''(\eta)] \\ &\quad - {H_a}^2 f''(\eta) = 0 \end{aligned} \qquad (11)$$

$$\begin{aligned} &\Theta'' + (N_b)(\Theta'\varphi') + (N_t){\Theta'}^2 \\ &\quad + (P_r E_c)\left(1+\frac{1}{\beta}\right) * \\ &\quad \left({f''}^2 + 4\delta^2 {f'}^2\right) \\ &\quad + (P_r S)(f\Theta' \\ &\quad - \eta\Theta') + {H_a}^2 {f'}^2(\eta) = 0 \end{aligned} \qquad (12)$$

$$\begin{aligned} &\varphi'' + (S_c S)(f\varphi' - \eta\varphi') + \left(\frac{N_t}{N_b}\right)\Theta'' \\ &\quad - S_c G_r \varphi = 0 \end{aligned} \qquad (13)$$

The boundary condition in the new similar variables becomes:

$$\begin{aligned} &f''(0) = 0 \, , f(0) = 0 \, , \theta'(0) = 0 \; , \\ &\varphi'(0) = 0 \quad at \quad \eta = 0 \end{aligned} \qquad (14)$$

$$f'(1) = 0 \, , f(1) = 1 \, , \theta(1) = \varphi(1) = 1 \quad at \qquad (15)$$

$$\eta = 1$$

Where S is the squeeze number, H_a is the Hartmann number, N_b is the Brownian motion parameter,N_t is the thermophoretic parameter, P_r is the Prandtl number,$S_c$is the Schmidt number andG_r the chemical reaction parameter which are defined as:

$$S = \frac{\alpha l^2}{2\upsilon} \, , P_r = \frac{\mu c_p}{K} \, , E_c = \frac{1}{c_p}\left(\frac{\alpha x}{2(1-\alpha t)}\right)^2 ,$$

$$\delta = \frac{l}{x} , N_b = \frac{(\rho c_p)_p D_B (C_H)}{(\rho c_p)_K} ,$$

$$N_t = \frac{(\rho c_p)_p D_T (T_H)}{((\rho c_p)_f K)} . H_a = \sqrt{\frac{l^2\sigma}{\mu}} B_0^2 , S_c = \frac{\upsilon}{D_B} , G_r = \frac{g l^2}{\upsilon}$$

It is important to note that the movement of the plates is described by squeezing number S ($S > 0$ is known as a "squeezing flow" and denotes that the plates are moving apart, whereas $S < 0$ denotes that the plates are moving together, [20], [21]. Moreover, it should be noted that $E_c = 0$ and $H_a = 0$, corresponds to the situation in which there is no magnetic force effect or viscous dissipation. While $G_r > 0$ represents the destructive chemical reaction and $G_r < 0$ characterizes the generative chemical reaction, the Prandtl number is used to assess the velocity at which momentum and energy propagate through the nanofluid and the Schmidt number is used to characterize fluid flows in which momentum and mass transfer processes are occurring simultaneously, [22].

The skin friction coefficient, Nusselt number, and Sherwood number are physical parameters of engineering relevance that are defined as:

$$C_f^* = \frac{\mu}{\rho v_w^2}\left(1+\frac{1}{\beta}\right)\left.\frac{\partial u}{\partial y}\right|_{y=h(t)} \qquad (16)$$

$$Nu^* = -\left(\frac{lK\left.\frac{\partial T}{\partial y}\right|_{y=h(t)}}{KT_H}\right) \qquad (17)$$

$$Sh^* = -\left(\frac{\mathrm{lD_B}\left.\frac{\partial \mathrm{c}}{\partial \mathrm{y}}\right|_{\mathrm{y=h(t)}}}{\mathrm{D_B C_H}}\right) \qquad (18)$$

Using variables **(9)**, after the simplification we get the skin friction coefficient and Nusselt, Sherwood numbers:

$$\begin{aligned} C_f &= \left(1+\frac{1}{\beta}\right) f''(1) \\ N_u &= -\theta'(1) \end{aligned} \qquad (19)$$

$$S_h = -\varphi'(1)$$

3 Homotopy Perturbation Technique

To illustrate the basic ideas of this method, we consider the following equation:

$$A(u) - f(r) = 0, \quad r \in \Omega \tag{20}$$

With the boundary condition of:

$$B\left(u, \frac{\partial U}{\partial n}\right) = 0, \quad r \in \Gamma \tag{21}$$

Where A is a general differential operator, B a boundary operator, $f(r)$ a known analytical function and
Γ is the boundary of the domain Ω.
A can be divided into two parts which are L and N, where L is linear and N is nonlinear.
Eqn. **(16)** can, therefore, be rewritten as follows:

$$L(u) + N(u) - f(r) = 0 \tag{22}$$

Homotopy perturbation structure is shown as follows:

$$H(v,p) = (1-p) * [L(v) - L(u_0)] + p[L(v) + N(v) - f(r)] = 0 \tag{23}$$

Were,

$$v(r,p): \Omega \times [0,1] \to R \tag{24}$$

In Eq. **(19)**, p belongs to [0, 1] is an embedding parameter and v_0 is the first approximation that satisfies the boundary condition. We can assume that the solution to Eq. **(21)** can be written as a power series in $\boldsymbol{p}$, as follows:

$$v = v_0 + pv_1 + p^2 v_2 + p^3 v_3 + \cdots \tag{25}$$

The best approximation for the solution is:

$$u = \lim_{p \to 1} v = v0 + v1 + v2 + \cdots \tag{26}$$

Applying the HPM to the problem, the equations are rewritten as follows:

$$H(f,p) = (1-p) * \left[\left(1+\frac{1}{\beta}\right) f'''' - \left(1+\frac{1}{\beta}\right) {f_0}''''(0)\right] + p[f'''' + S(ff''' - 3f'' - \eta f''' - f'f'') - Ha^2 f''] = 0 \tag{27}$$

$$H(\theta,p) = (1-p)[\Theta'' - {\Theta_0}''(0)] + p\left[\begin{array}{c} \Theta'' + (N_b)(\Theta'\varphi') + (N_t)\Theta'^2 + \\ (P_r E_c)\left(1+\frac{1}{\beta}\right)\left(f''^2 + 4\delta^2 f'^2\right) + \\ (P_r S)(f\Theta' - \eta\Theta') + {H_a}^2 f'^2(\eta) \end{array}\right] = 0 \tag{28}$$

$$H(0,\varphi) = (1-p)[\varphi'' - {\varphi_0}''(0)] + p\left[\varphi'' + (S_c S)(f\varphi' - \eta\varphi') + \left(\frac{N_t}{N_b}\right)\Theta'' - S_c G_r \varphi\right] \tag{29}$$

We consider f and θ as follows:

$$f(\eta) = f_0(\eta) + p^1 f_1(\eta) + p^2 f_2(\eta) + p^3 f_3(\eta) + \cdots = \sum_{i=0}^{N} p^i f_i(\eta) \tag{30}$$

$$\theta(\eta) = \theta_0(\eta) + p^1 \theta_1(\eta) + p^2 \theta_2(\eta) + p^3 \theta_3(\eta) + \cdots = \sum_{i=0}^{N} p^i f_i \theta_i(\eta) \tag{31}$$

(32)

With substituting f, θ and φ from equations **(26-28)** into equations **(10-12)** and some simplification and rearranging based on powers of $p-terms$, we have:

$$p^0: \quad {f_0}'''' = 0, \quad {\theta_0}'' = 0, \quad {\varphi_0}'' = 0 \tag{33}$$

$$f''(0) = 0, \quad f(0) = 0, \theta'(0) = 0, \quad \phi'(0) = 0 \quad at \quad \eta = 0 \tag{34}$$

$$f'(1) = 0, f(1) = 1, \quad \theta(1) = \phi(1) = 1 \quad at \quad \eta = 1 \tag{35}$$

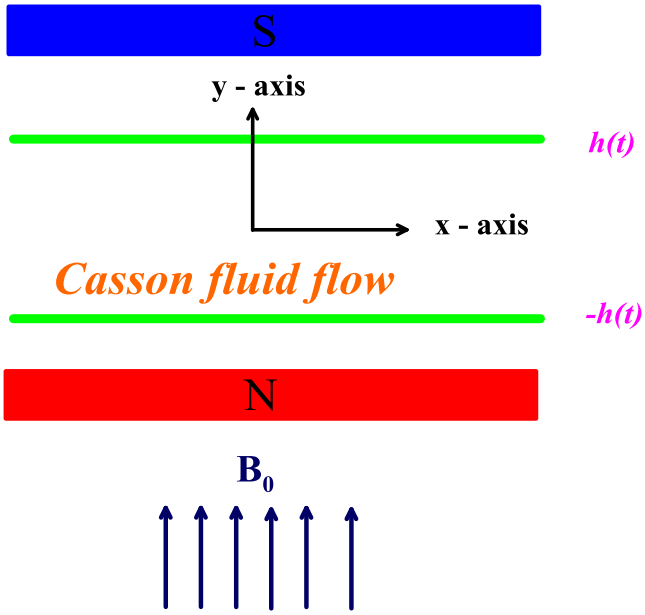

Fig. 1: Geometry of the problem

$$
\begin{aligned}
&p^1: \\
&f_1'''' + S(f_0 f_0''' - 3f_0'' - \eta f_0''' - f_0' f_0'') \\
&\quad -Ha^2 f_0'' = 0 \\
&\theta_1'' + (P_r E_c)\left(f_0''^2 + 4\delta^2 f_0'^2\right) \\
&\quad + (P_r S)(f_0 \theta_0' - \eta\theta_0') \\
&\quad + (N_b)(\theta_0' \varphi_0') \\
&\quad + (N_t)\theta_0'^2 + H_a^2 f_0'^2(\eta) \\
&\quad = 0 \\
&\varphi_1'' + (S_c S)(f_0 \varphi_0' - \eta\varphi_0') + \left(\frac{N_t}{N_b}\right)\theta_0'' \\
&\quad - S_c G_r \varphi_0 = 0
\end{aligned}
\tag{36}
$$

The boundary conditions are:

$$
\begin{aligned}
&f_1''(0) = 0, f_1(0) = 0, \\
&\theta_1'(0) = 0\,, \varphi_1'(0) = 0 \quad at \\
&\eta = 0
\end{aligned}
\tag{37}
$$

$$
\begin{aligned}
&f_1'(1) = 0, f_1(1) = 0, \\
&\theta_1(1) = 0\,, \varphi_1(1) = 0 \quad at \\
&\eta = 1
\end{aligned}
\tag{38}
$$

Solving the above equations with their corresponding boundary conditions using maple we would obtain:

$$
\begin{aligned}
f_0(\eta) &= -\frac{1}{2}\eta^3 + \frac{3}{2}\eta \\
\theta_0(\eta) &= 1 \\
\varphi_0(\eta) &= 1
\end{aligned}
\tag{39}
$$

The terms $f_i(\eta)$, $\theta_i(\eta)$ and $\varphi_i(\eta)$ when $i \geq 1$ is too large that is mentioned graphically. The solution of equations is obtained when $p \to l$, will be as follows:

$$
\begin{aligned}
f(\eta) &= f_0(\eta) + p^1 f_1(\eta) + p^2 f_2(\eta) \\
&\quad + p^3 f_3(\eta) + \cdots \\
&= \sum_{i=0}^{N} p^i f_i(\eta)
\end{aligned}
\tag{40}
$$

$$
\begin{aligned}
\theta(\eta) &= \theta_0(\eta) + p^1 \theta_1(\eta) + p^2 \theta_2(\eta) \\
&\quad + p^3 \theta_3(\eta) + \cdots \\
&= \sum_{i=0}^{N} p^i f_i \theta_i(\eta)
\end{aligned}
\tag{41}
$$

$$
\begin{aligned}
\varphi(\eta) &= \varphi_0(\eta) + p^1 \varphi_1(\eta) + p^2 \varphi_2(\eta) \\
&\quad + p^3 \varphi_3(\eta) + \cdots \\
&= \sum_{i=0}^{N} p^i \varphi_i(\eta)
\end{aligned}
\tag{42}
$$

- **Validation of code**

To answer the problem, HPM and RK-4 are used in the current paper. As can be seen in Table 1, the current codes are validated by contrasting the acquired findings with the previously published results in the literature. This comparison shows that the codes provide a very precise answer to this issue. The findings show excellent agreement.

Table 1. *Comparison between Present and Mustafa et al, Dogonchi et al results for* $-f''(1)$ *and* $-\theta'(1)$ *when* $E_c = P_r = S_c = G_r = 1, H_a = 0$ *and* $\delta = 0.1$ *for different values of* S

S	Ref [4]		Ref [5]		Present results			
	HAM		DRA		HPM		NM	
	$-f''(1)$	$-\theta'(1)$	$-f''(1)$	$-\theta'(1)$	$-f''(1)$	$-\theta'(1)$	$-f''(1)$	$-\theta'(1)$
-1.0	2.170090	3.319899	2.170091	3.319888	2.170092	3.319860	2.170090	3.319899
-0.5	2.614038	3.129491	2.617403	3.129491	2.617403	3.129491	2.617403	3.129491
0.01	3.007134	3.047092	3.007133	3.047091	3.007133	3.047091	3.007133	3.047091
0.5	3.336449	3.026324	3.336449	3.026323	3.336449	3.026323	3.336449	3.026323
2.0	4.167389	3.118551	4.167041	3.113386	4.168065	3.127819	4.167389	3.118550

4 Discussion of Results

The results are interpreted in graphs and tables for various values of relevant factors to aid in better clarity and comprehension of the issue. Figure 2, Figure 3, Figure 4 and Figure 5 show how squeezing number $(\mp S)$ affects velocity, temperature, and concentration profiles. It's important to note that all figures are depicted for the expanding flow scenario $(S > 0)$ and the squeezing flow case $(S < 0)$. Figure 2, Figure 3, Figure 4 and Figure 5 demonstrate that the impact of positive and negative squeezing numbers differs: According to Figure 2, the normal velocity profile becomes higher for $S < 0$ and lowers for $S > 0$. This is because as plates separate, fluid is drawn into the channel, increasing the velocity field. In a different scenario, liquid within the channel is released when plates move near one another. This results in a liquid drop inside the channel and a decrease in fluid velocity. Squeezing number, however, depends on the flow region's velocity field. Furthermore, as seen in Figure 3, the axial flow velocity profile increased in the remaining half for rising values of $S > 0$ and dropped in the area $0 \leq \eta \leq 0.45$. Conversely, with rising values of S < 0, it drops in the remaining section and increases in the region $0 \leq \eta \leq 0.45$. For $S > 0$, the concentration profile rises, and the temperature field continues to decrease in Figure 4 and Figure 5. In contrast, the concentration profile decays, and the temperature field grows when $S > 0$. The greater distance between the plates is the cause of the temperature field's drop, which can be related to a decrease in kinematic viscosity or an increase in the speed at which the plates travel.

Similarly, Figure 6, Figure 7, Figure 8 and Figure 9 show how the Hartman number affects temperature, velocity, and concentration curves. The pictures illustrate how the normal velocity profile in Figure 6 reduces as Hartman number Ha grows because of the existence of Lorentz forces acting against the flow, which causes resistance to flow to occur and a corresponding decrease in the velocity field. Additionally, Figure 7 shows that the axial velocity field rises in the remaining portion and decreases in the area $0 \leq \eta \leq 0.45$. However, Figure 8 shows that the temperature field increases. Additionally, it can be shown in Figure 9 that the concentration increases.

Similarly, Figure 10, Figure 11, Figure 12 and Figure 13 show how the Casson fluid parameter β affects temperature, concentration, and velocity profiles. As the Casson fluid parameter β grows, the normal velocity drops, as seen in Figure 10. This is because the applied stresses cause the slight increase in β to increase the viscosity of the nanofluid, which in turn causes the normal velocity to decrease. Furthermore, Figure 11 shows that the axial velocity profile increases in the remaining section while decreasing in the portion $0 \leq \eta \leq 0.45$. Additionally, the temperature field drops in Figure 12 and the concentration rises in Figure 13.

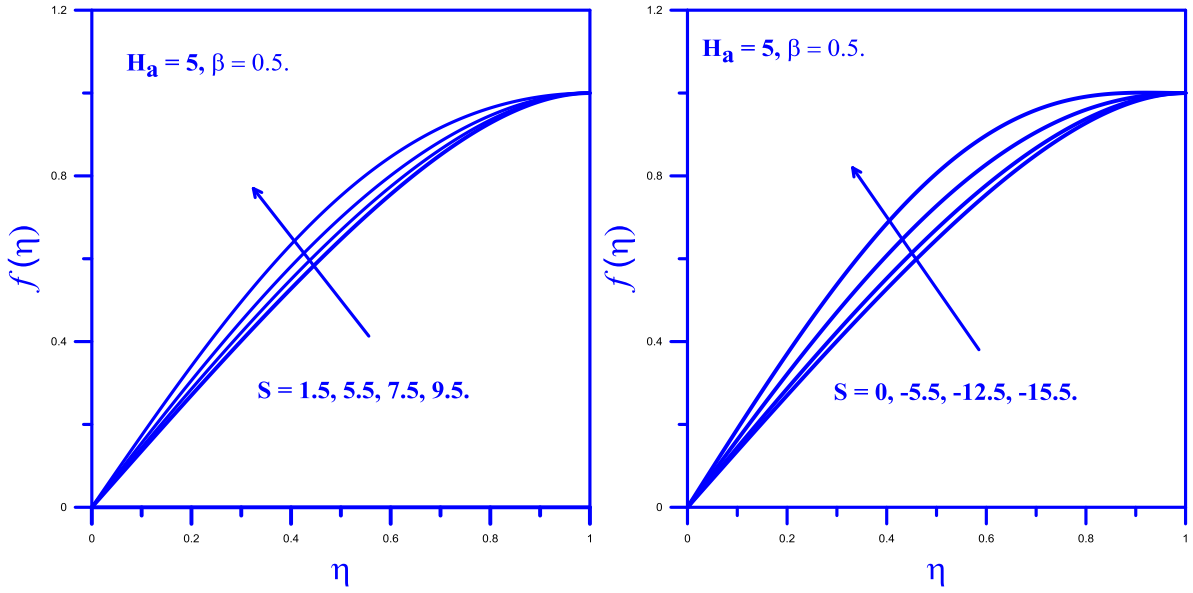

Fig. 2: *impact of* $\mp S$ *on* $f(\eta)$

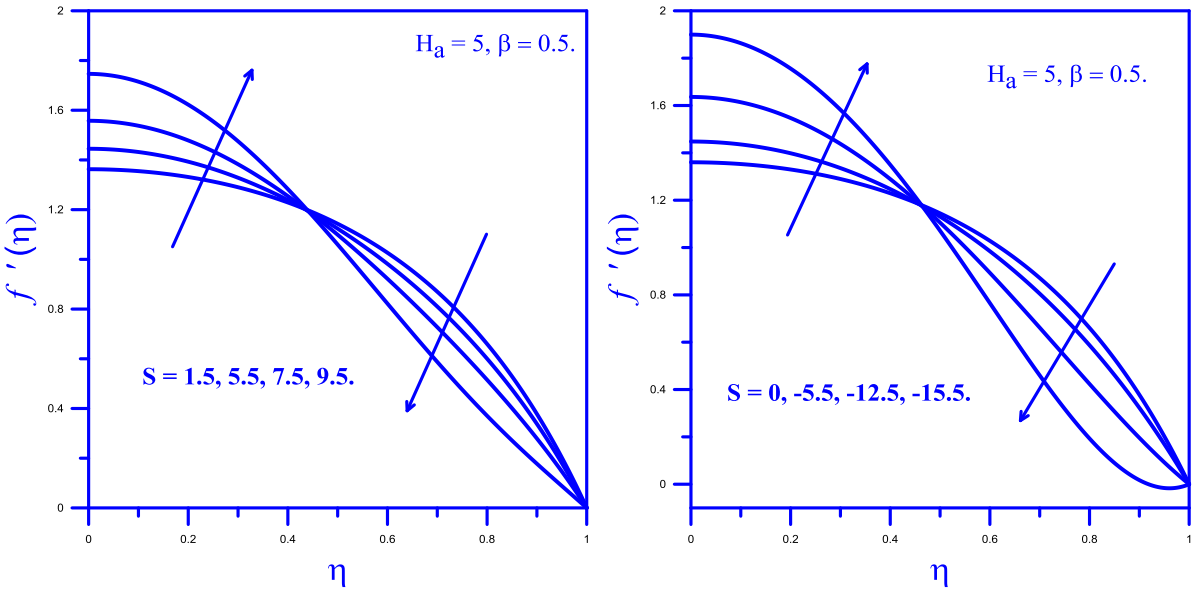

Fig. 3: impact of $\mp$ S on f′(η)

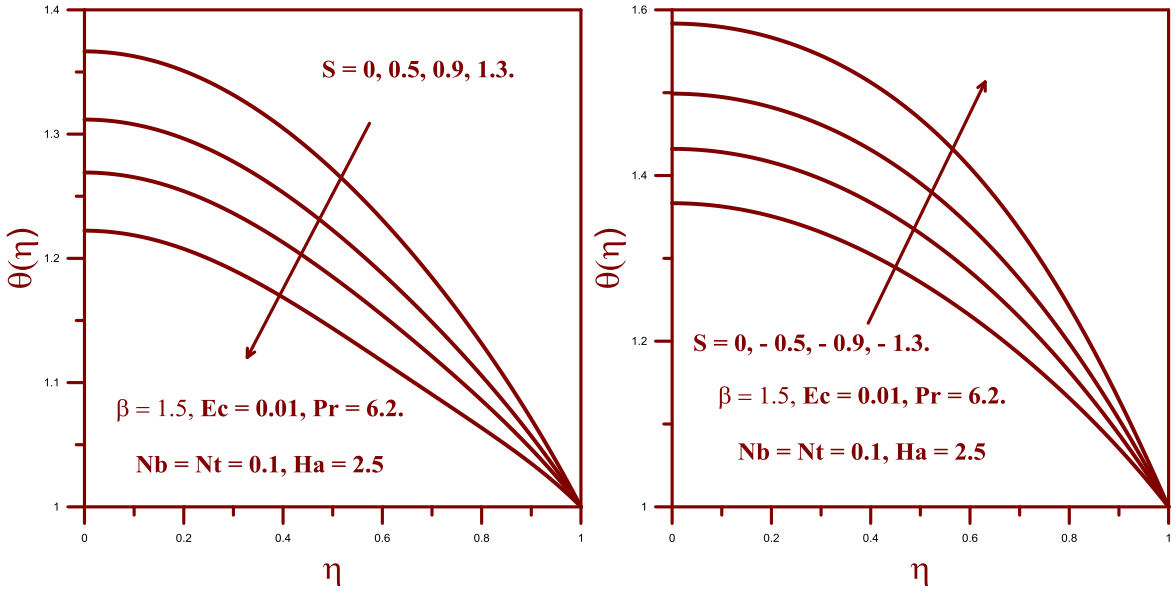

Fig. 4: impact of $\mp$ S on θ(η)

Figure 14 and Figure 15 show the effects of the Brownian motion parameter N_b and the thermophoresis parameter N_t on the concentration profile. It is evident from Figure 14 that when N_t increases, the concentration profile diminishes. Stronger thermophoresis forces that have emerged in the flow zone are the cause of this condition. In contrast, Figure 15 shows that it rises with N_b.

Figure 16 and Figure 17 show how the time-dependent chemical reaction parameters G_r and Schmidt number S_c affect the concentration profile.

Figure 16 shows that the concentration profile is affected differently by both positive and negative time-dependent chemical reaction parameters. The concentration profile decreases for $G_r > 0$ due to the chemical reaction's breakdown. Conversely, it rises when $G_r < 0$ because of the chemical reaction. In contrast, the concentration distribution decreases as S_c rises in Figure 17.

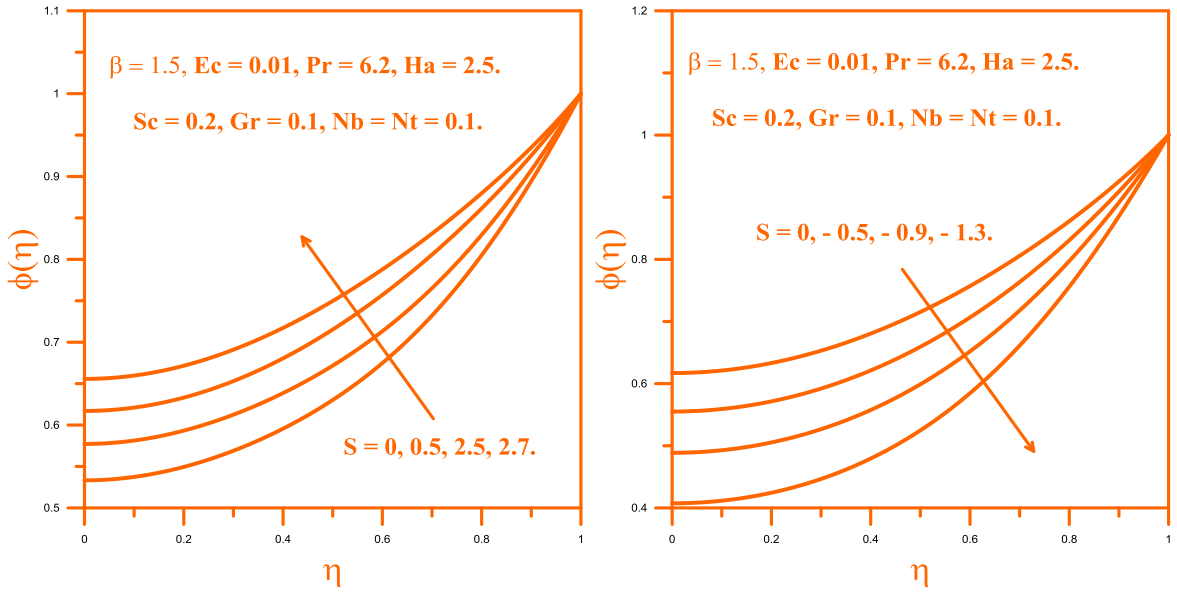

Fig. 5: impact of $\mp$ S on $\phi(\eta)$

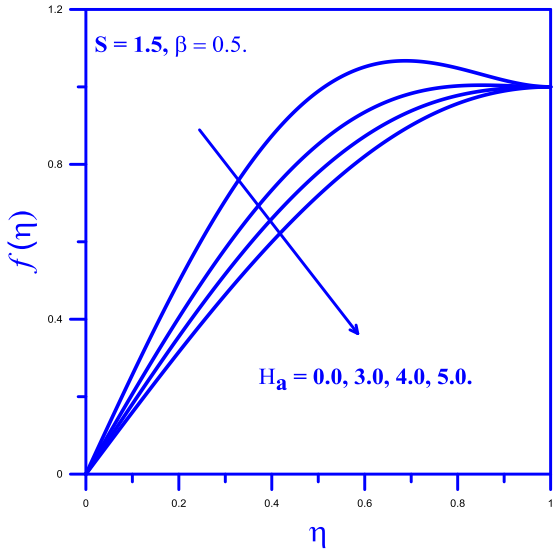

Fig. 6: *impact of* H_a *on* $f(\eta)$

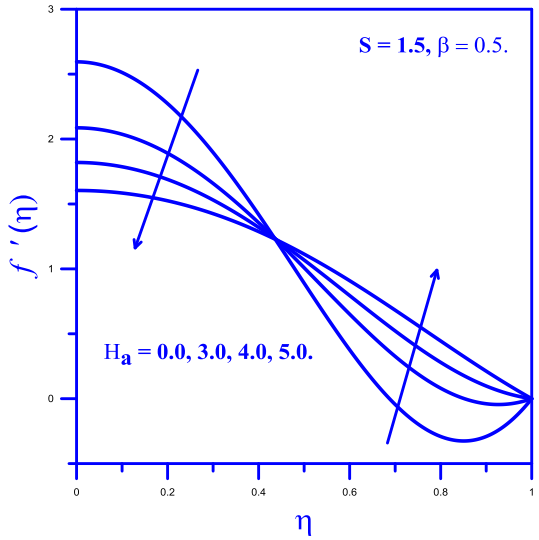

Fig. 7: *impact of* H_a *on* $f'(\eta)$

The Skin Friction coefficient C_f, Nusselt number N_u, and Sherwood number S_h were found to vary with the Squeeze number S, Casson parameter β, and Hartman number H_a in Table 2. It is evident from Table 2 that as S and $H_a$values rise, the skin friction coefficient drops, and when β values rise, it rises. Additionally, Tab. 3 shows that the Nusselt number rises for H_a but falls for growing values of S and β. Additionally, Table 2 demonstrates that the Sherwood number rises as S and β values rise while falling as H_a values rise.

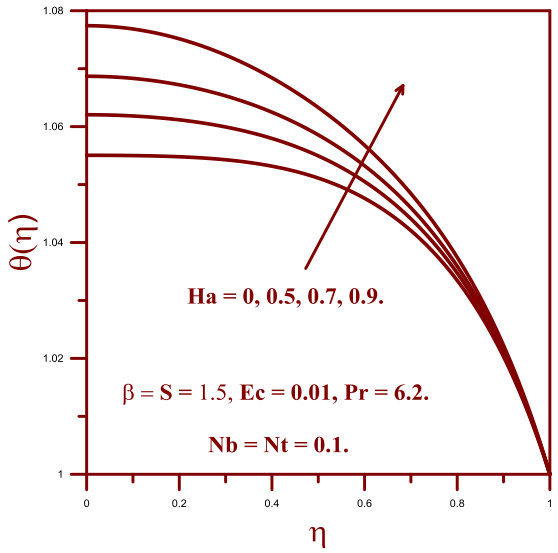

Fig. 8: *impact of* H_a *on* $\theta(\eta)$

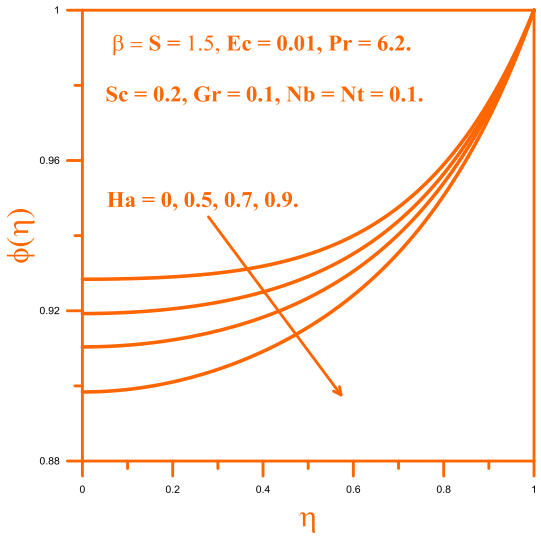

Fig. 9: *impact of* H_a *on* $\phi(\eta)$

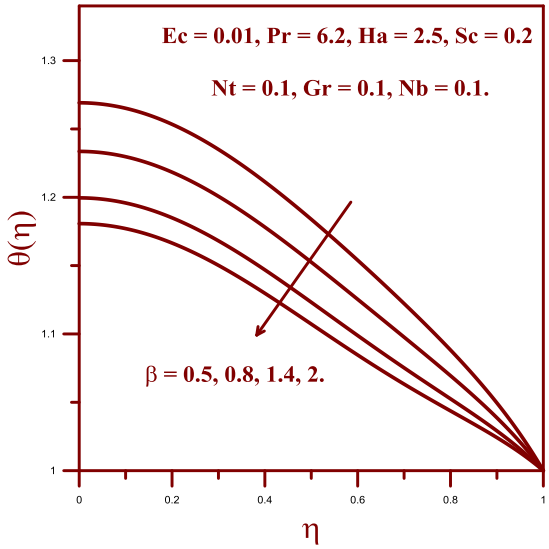

Fig. 12: *impact of* β *on* $\theta(\eta)$

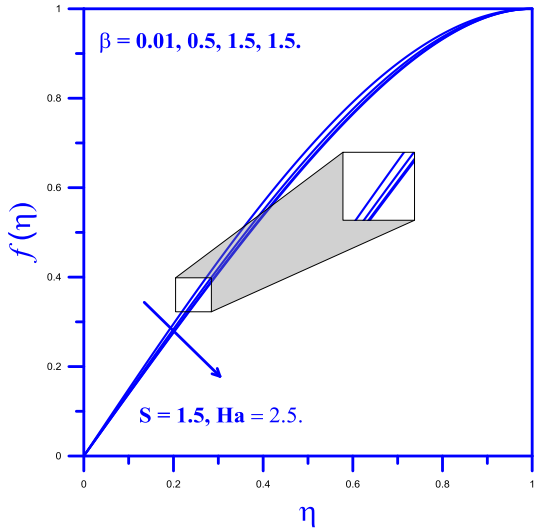

Fig. 10: *impact of* β *on* $f(\eta)$

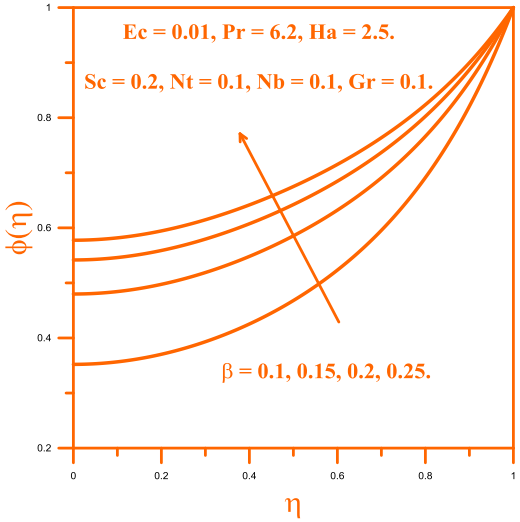

Fig. 13: *impact of* β *on* $\phi(\eta)$

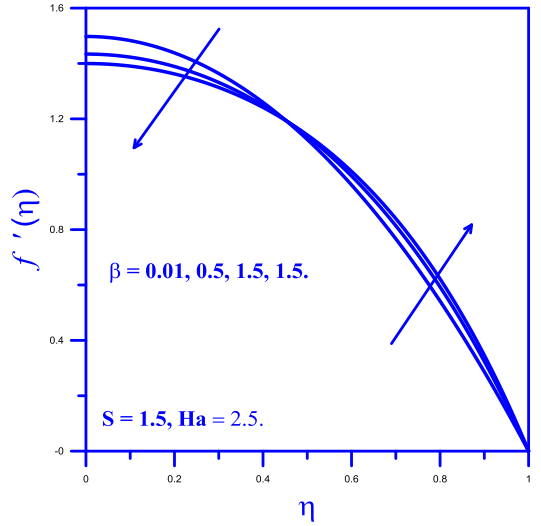

Fig. 11: *impact of* β *on* $f'(\eta)$

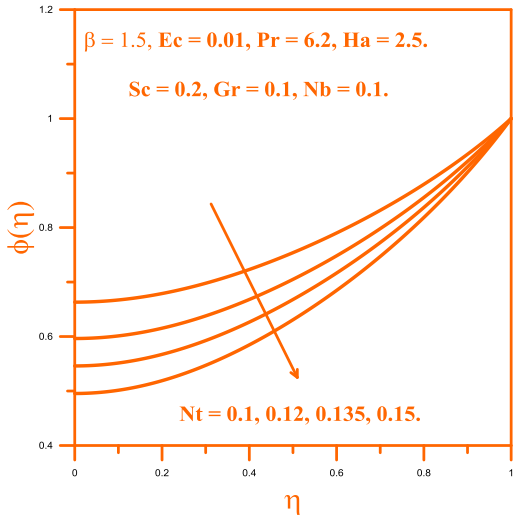

Fig. 14: *impact of* N_t *on* $\phi(\eta)$

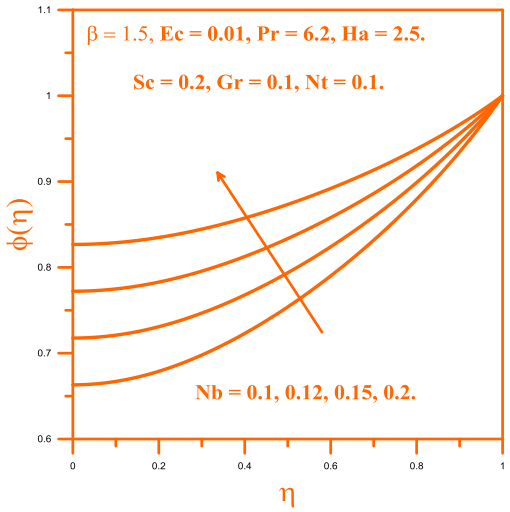

Fig. 15: impact of N_b on $\phi(\eta)$

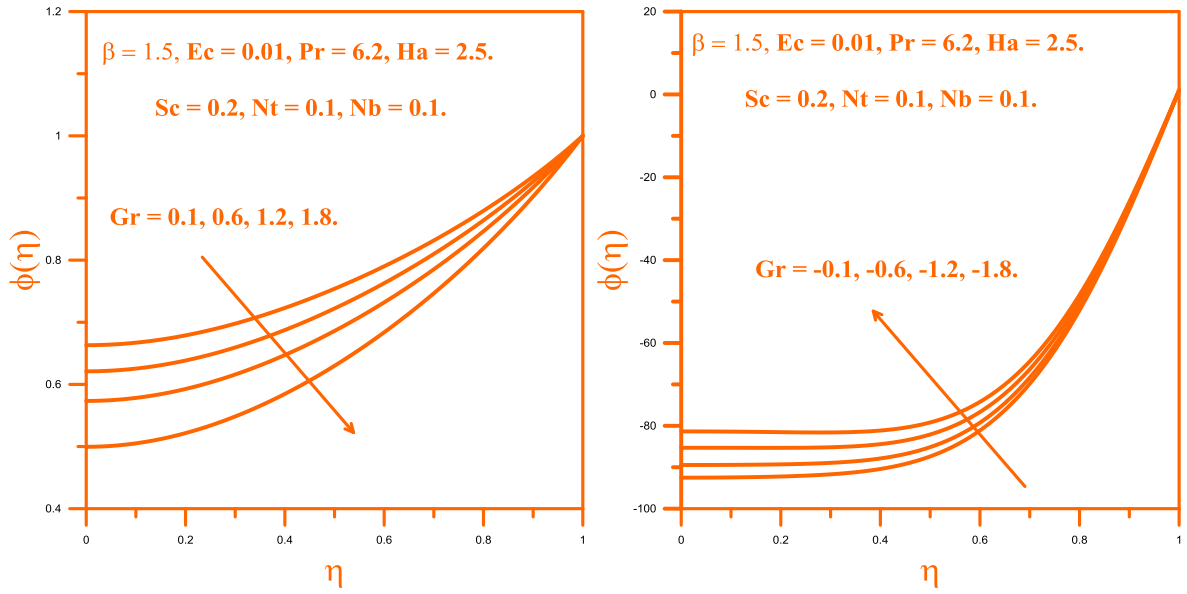

Fig. 16: *impact of* $\mp G_r$ *on* $\phi(\eta)$

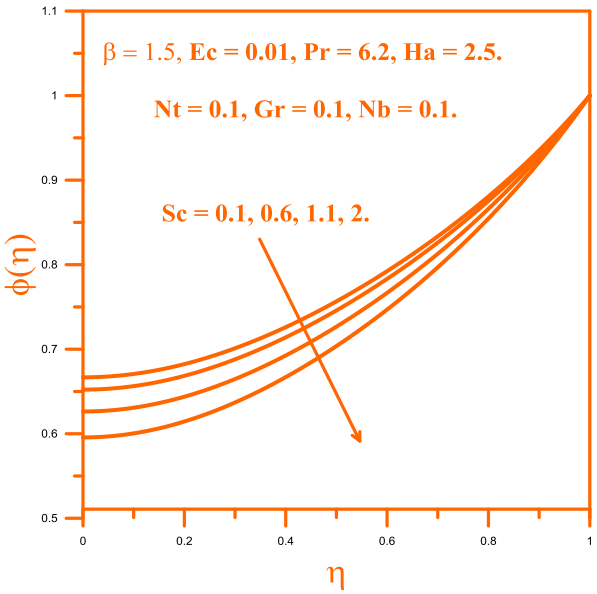

Fig. 17: *impact of* S_c *on* $\phi(\eta)$

Table 2. Skin friction, Nusselt number and Sherwood number coefficients for different values of S, β and H_a when $N_b = 0.1, N_t = 0.1$ $E_c = 0.01, G_r = 0.1, P_r = 6.2$, $S_c = 0.5$.

S	β	H_a	$C_f = \left(1 + \frac{1}{\beta}\right) f''(1)$	$N_u = -\theta'(1)$	$S_h = -\varphi'(1)$
-1	1	2	-6.0858218460	1.0113136395	-1.0622791120
-0.5			-6.4318509673	0.8088745369	-0.8655341258
0.0			-6.7579586889	0.6703420350	-0.7247119376
0.5			-7.0665588433	0.5707471689	-0.6398027050
1.0			-7.3592614969	0.4851209735	-0.6107965858
0.5	0.5		-10.094364079	0.7422135661	-0.8106079572
	1.0		-7.0665588433	0.5707471689	-0.6398027050
	1.5		-6.0507360057	0.5130723151	-0.5845460590
	1	0.0	-6.3462955265	0.3484822973	-0.3954251196
		0.5	-6.3934787417	0.3626192293	-0.4099299356
		1.0	-6.5332004275	0.4048828001	-0.4540328386

5 Conclusion

In the presence of a uniform magnetic field, this study investigates the impact of thermophoresis and Brownian motion on the heat and mass transfer of a two-phase, unstable squeezing flow of MHD Casson nanofluid with time-dependent chemical reaction. The governing equations are solved using HPM, and the correctness of our solutions is confirmed using a shooting method and the fourth order Runge-Kutta approach. Therefore, the previously published study and the analytical and numerical results agreed in a fascinating way, as expected. Furthermore, the impacts of additional significant variables have been examined and displayed in tables and graphs, accordingly. The current study has led to the following significant findings:

- When $S > 0$, the velocity field is suppressed; for $S < 0$, it is augmented.
- When $S > 0$, the temperature profile falls, and when $S < 0$, it rises. On the other hand, the concentration field shows the opposite tendency.
- As β increases, the velocity field decreases. Additionally, when β grew, the temperature profile decreased, and the concentration profile rose.
- Concentration and velocity fields get smaller when the values of H_a . In contrast, the temperature profile rises with the values of H_a .
- As the thermophoresis parameter increases, the concentration field shrinks.
- As the Brownian motion parameter increases, the concentration profile rises.
- Concentration field ultimately becomes strengthened for $G_r > 0$ and S_c and eventually muted for $G_r < 0$.

References:

[1] Stefan MJ. Versuch Uber die scheinbare adhesion. Academic der Wissenschaften in Wien. *Mathematik-Naturwissen*. 1874; 69: 713–721.

[2] G. Domairry, A. Aziz; Approximate analysis of MHD squeeze flow between two parallel disks with suction or injection by homotopy perturbation method; *Math. Prob. Eng*. (2009), pp. 603–616.

[3] Mahmood M, Asghar S, Hossain MA (2007) Squeezed flow and heat transfer over a porous surface for viscous fluid. *Heat Mass Transf* 44:165–173.

[4] M. Mustafa, T. Hayat, S. Obaidat; On heat and mass transfer in the unsteady squeezing flow between parallel plates; *Mechanica*, 47 (2012), pp. 1581–1589.

[5] Dogonchi AS, Ganji DD. Investigation of MHD nanofluid flow and heat transfer in astretching/shrinking convergent/divergent channel considering thermal radiation. *J. Of Molecular Liquids*. 2016; 220: 592-603.

[6] M. Sheikholeslami, Sh. Abelman, D.D.Ganji: Numerical simulation of MHD nanofluid flow and heat transfer considering viscous dissipation. *International Journal of heat and mass transfer*, 79(2014)212-222.

[7] McDonald, D. A. *Blood flow in arteries*. 1974. Edward Arnold, London, 92-95.

[8] Eldabe, N. T. M., Saddeck, G., & El-Sayed, A. F. (2001). Heat transfer of MHD non-

Newtonian Casson fluid flow between two rotating cylinders. *Mechanics and Mechanical Engineering*, 5(2), 237-251.

[9] Boyd, J., Buick, J. M., & Green, S. (2007). Analysis of the Casson and Carreau-Yasuda non-Newtonian blood models in steady and oscillatory flows using the lattice Boltzmann method. *Physics of Fluids*, 19(9), 093103.

[10] Mustafa, M., Hayat, T., Pop, I. and Aziz, A. (2011) Unsteady Boundary Layer Flow of a Casson Fluid Due to an Impulsively Started Moving Flat Plate. *Heat Transfer-Asian Research*, 40, 563-576. http://dx.doi.org/10.1002/htj.20358.

[11] Fredrickson, A. G. (1964). *Principles and applications of rheology*. Prentice-Hall.

[12] M. Sheikholeslami, M. Azimi, D.D. Ganji; Application of differential transformation method for nanofluid flow in a semi-permeable channel considering magnetic field effect; *J. Comput. Meth. Eng. Sci. Mech.*, 16 (2015), pp. 246–255.

[13] M.J. Jang, C.L. Chen, Y.C. Lin; Two-dimensional differential transformation method for solving partial differential equation; *Appl. Math. Comput.*, 121 (2001), pp. 261–270.

[14] S.T. Mohyud-Din, A. Yildirim; Variation of parameter method for Fisher's equation; *Adv. Appl. Math. Mech.*, 2 (2010), pp. 379–388.

[15] M. Sheikholeslami, R. Ellahi, H.R. Ashorynejad, T. Hayat; Effects of heat transfer in flow of nanofluids over a permeable stretching wall in a porous medium; *J. Comput. Theor. Nanosci.*, 11 (2014), pp. 486–496.

[16] M. Sheikholeslami, D.D. Ganji, H.R. Ashorynejad; Investigation of squeezing unsteady nanofluid flow using ADM; *Powder Technol.*, 239 (2013), pp. 259–265.

[17] M. Sheikholeslami, D.D. Ganji; Heat transfer of Cu-water nanofluid between parallel plates; *Powder Technol.*, 235 (2013), pp. 873–879.

[18] He, J. H. (2000). A new perturbation technique which is also valid for large parameters. *Journal of Sound and Vibration*, 229(5), 1257-1263.

[19] Rohlf, K., &Tenti, G. (2001). The role of the Womersley number in pulsatile blood flow: a theoretical study of the Casson model. *Journal of biomechanics*, 34(1), 141-148.

[20] Lohmann, T., Bock, H. G., &Schloeder, J. P. (1992). Numerical methods for parameter estimation and optimal experiment design in chemical reaction systems. *Industrial & engineering chemistry esearch*, 31(1), 54-57.

[21] Rapp, B. E. (2016). *Microfluidics: modeling, mechanics, and mathematics*. William Andrew.

[22] Sheikholeslami, M., & Ganji, D. D. (2016). *External magnetic field effects on hydrothermal treatment of nanofluid: numerical and analytical studies*. William Andrew.

Contribution of Individual Authors to the Creation of a Scientific Article (Ghostwriting Policy)

- A. EL Harfouf: Conceptualization, Formal analysis, Investigation, Methodology, Project administration, Resources, Validation, Writing – original draft, Data curation, Software, Visualization.
- R. Herbazi: Conceptualization, Formal analysis, Investigation, Methodology, Project administration, Resources, Validation, Writing – review & editing.
- S. Hayani Mounir: Conceptualization, Investigation, Project administration, Writing – review & editing.
- H. Mes-adi: Conceptualization, Formal analysis, Investigation, Methodology, Project administration, Resources, Validation, Writing – review & editing.
- A. Wakif: Conceptualization, Investigation, Project administration, Supervision, Writing – review & editing.

Sources of Funding for Research Presented in a Scientific Article or Scientific Article Itself

No funding was received for conducting this study.

Conflict of Interest

The authors have no conflicts of interest to declare.